Three-Dimensional Momentum Imaging of Electron Wave Packet Interference in Few-Cycle Laser Pulses

R. Gopal, K. Simeonidis, R. Moshammer, Th. Ergler, M. Dürr, M. Kurka, K.-U. Kühnel, S. Tschuch, C.-D. Schröter, D. Bauer, and J. Ullrich

Max-Planck-Institut für Kernphysik, Saupfercheckweg 1, D-69117 Heidelberg, Germany

A. Rudenko

Max-Planck Advanced Study Group at CFEL, D-22607 Hamburg, Germany

O. Herrwerth, Th. Uphues, M. Schultze, E. Goulielmakis, M. Uiberacker, M. Lezius, and M. F. Kling

Max-Planck-Institut für Quantenoptik, Hans-Kopfermann-Strasse 1, D-85748 Garching, Germany

(Received 10 February 2009; published 27 July 2009)

Using a reaction microscope, three-dimensional (3D) electron (and ion) momentum (**P**) spectra have been recorded for carrier-envelope-phase (CEP) stabilized few-cycle (~5 fs), intense ($\sim 4 \times 10^{14}$ W/cm^2) laser pulses (740 nm) impinging on He. Preferential emission of low-energy electrons ($E_e < 15$ eV) to either hemisphere is observed as a function of the CEP. Clear interference patterns emerge in **P** space at CEPs with maximum asymmetry, interpreted as attosecond interferences of rescattered and directly emitted electron wave packets by means of a simple model.

DOI: 10.1103/PhysRevLett.103.053001 PACS numbers: 32.80.Rm

Ionization of rare gas atoms such as helium at laser intensities in the range of 10^{14}–10^{15} W/cm^2 is usually described by tunneling, where the valence electron tunnels through the field suppressed barrier. The electron then undergoes an oscillatory motion in the electric field to achieve a final momentum, also known as the drift momentum. In few-cycle pulses (e.g., 5 fs at 800 nm with a single cycle time period of 2.7 fs), a highly nonlinear process such as tunneling is confined to a single cycle around the maximum of the pulse envelope, as illustrated in Fig. 1. Here, for a sinelike waveform ($\phi_{\mathrm{CEP}} = \pm\pi/2$, CEP: carrier-envelope-phase, defined as the phase difference between the envelope maximum and the nearest electric field maximum), two tunneling phases, symmetrically spaced around the zero crossing of the field will lead to the same momentum, and the corresponding trajectories will interfere. As first outlined in [1] and detailed in [2], the wave packet EWP_1 that was launched at t_1 recollides with the ionic core thereby being modified in phase and wavefront direction (often dubbed "Coulomb focusing") and overlaps with an unaffected "reference" wave EWP_2 (of the same electron) launched at t_2. A 3D momentum image of these electron wave-packet (EWP) interferences therefore represents a time-dependent hologram of the modulations imposed onto EWP_1. Here the attosecond dynamics of the electron cloud bound to the ion might be imprinted and can potentially be reconstructed for atomic, molecular, and cluster targets. In experiments the interaction of the returning EWP_1 with the parent ion core has been used to retrieve atomic or molecular structure and dynamics through high harmonic generation, as for, e.g., in [3,4] or through electron diffraction as in [5]. More recently interferences with EWPs generated by attosecond pulse trains and steered by an infrared laser pulse [6] have been demonstrated to image the coherent scattering of electrons from the parent ion [7].

In this Letter we report on the first demonstration of subcycle EWP interferences seen in high-resolution, 3D low-energy electron (ion) momentum distributions for single ionization of He by CEP-stabilized few-cycle pulses, investigated by a "reaction microscope" [8]. Momentum distributions along the laser polarization axis ($p_\parallel$), not only show a CEP-dependent preferential emission to either hemisphere, but also a corresponding asymmetric occurrence of interference peaks. The spacing between the peaks, significantly smaller than $\Delta p_\parallel \propto \sqrt{1\hbar\omega}$ as observed for longer pulses, is compared with a simple strong field

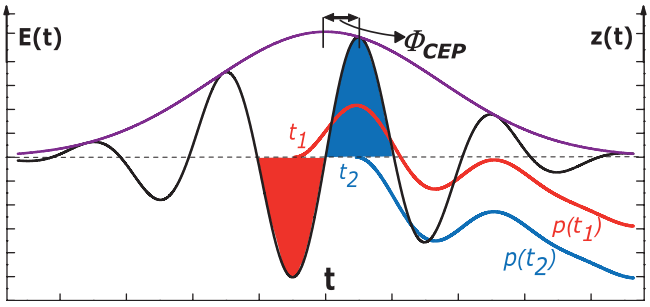

FIG. 1 (color). Electron trajectories in an ultrashort pulse, with $\phi_{\mathrm{CEP}} = \pi/2$. Electrons born at times t_s ($s = 1, 2$) end up with the same momentum $p(t_s)$ following the trajectories given by the red and blue curves, respectively: $p(t_s) = -\int_{t_s}^{\infty} E(t)dt$, in atomic units. The right-hand axis is the displacement of the electron from $z = 0$.

approximation (SFA)-based model. This model invokes the interference of only two quantum paths for wave packets EWP_1 and EWP_2 leading to the same final drift momentum, hence capturing the basic mechanism of holographic imaging. 2D electron spectra ($E_e < 15$ eV) reveal regular interference stripes, parallel to the transverse momentum ($p_\perp$) axis in the hemisphere of enhanced emission, and radial structures in the opposite hemisphere, in good qualitative agreement with theoretical predictions [2].

In the experiment, linearly polarized CEP-stabilized 5 fs pulses at 740 nm with a repetition rate of 3 kHz were obtained at the AS-1 attosecond beam line at Max Planck Institute for Quantum Optics [9]. The laser beam, with intensities up to 0.4 PW/cm^2 (I_0) at the focus of a 125 mm spherical Ag mirror was crossed with a supersonic, cold He jet ($\sim 10^{11}$ atoms/cm^2) in the ultrahigh vacuum chamber ($\sim 2 \times 10^{-10}$ mbar) of the reaction microscope. The created ions and electrons were guided to two position sensitive channel plate detectors by weak electric (~ 2 V/cm) and magnetic (~ 0.8 mT) fields, applied along the laser polarization axis. To avoid slipping of the Gouy phase [10] the focus of the laser was kept slightly before the actual jet position. Superior momentum resolution along the polarization axis (the spectrometer axis) was achieved reaching $\Delta p_\parallel < 0.02$ a.u. for both ions and electrons. Along the transverse directions (i.e., in the plane perpendicular to the laser polarization), the ion momentum resolution varied from ~ 0.5 a.u. along the gas jet direction to < 0.1 a.u. in the direction perpendicular to the jet. The transverse momentum resolution for electrons was on the level of 0.05 a.u. The CEP of the laser field was varied in steps over a range of 2π radians. For each of the phases, the two-dimensional position and time-of-flight spectra for the ions and electrons were recorded in coincidence, and thus 3D momentum distributions were obtained [8].

Depending on the CEP, the projections of the recoil-ion (electron) momentum distributions along the laser polarization axis show an asymmetry about $p_\parallel = 0$ which can be characterized through an asymmetry parameter, $a(\phi_{\mathrm{CEP}}) = (P_+(\phi_{\mathrm{CEP}}) - P_-(\phi_{\mathrm{CEP}}))/(P_+(\phi_{\mathrm{CEP}}) + P_-(\phi_{\mathrm{CEP}}))$. $P_\pm$ is simply the number of ions detected, which initially flew towards, or away from the detector and $a(\phi_{\mathrm{CEP}})$ indicates a "left-right" asymmetry [11]. While we do not measure the absolute CEP, we fix the phase $\phi_{\mathrm{CEP}} = 0$ for the CEP with the most symmetric distribution and in the inset of Fig. 2, plot $a(\phi_{\mathrm{CEP}})$ against ϕ_{CEP}. There is a clear progressive shift of the asymmetry from negative to positive and back, demonstrating the consistency of these measurements. In particular, a change of phase by π inverts the distribution $[a(\phi_{\mathrm{CEP}}) = -a(\phi_{\mathrm{CEP}} + \pi)]$, and a shift by 2π reproduces the original distribution $[a(\phi_{\mathrm{CEP}}) = a(\phi_{\mathrm{CEP}} + 2\pi)]$. Having identified the points of maximum (and opposite) asymmetry, we proceed to plot in Figs. 2(a) and 2(b) recoil-ion momentum distributions $p_\parallel$ for these phases. In Fig. 2(a), for $p_\parallel > 0$, we see peaks, which mostly disappear for $p_\parallel < 0$. When

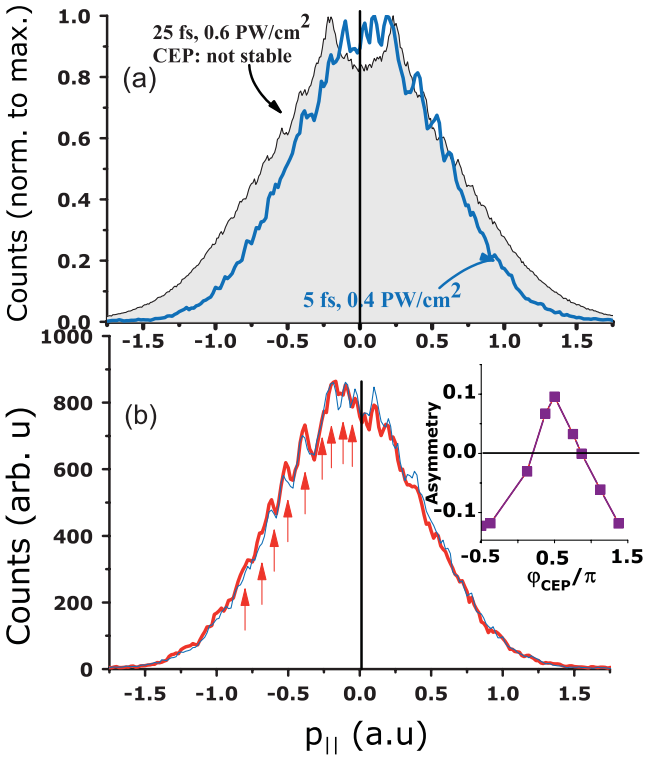

FIG. 2 (color). (a) Recoil-ion (He^+) momentum distributions along the laser polarization axis for CEP with maximum asymmetry towards positive momenta and (b) at $\phi_{\mathrm{CEP}} = \pi/2$. Shaded curve: ion momentum distribution at a similar intensity but for longer, 25 fs pulses normalized to the integral under the blue line. The thin blue curve in (b) is a mirror image of the blue curve in (a). Inset: asymmetry parameter $a(\phi_{\mathrm{CEP}})$ as a function of the relative CE phase (see text).

we change the phase by π in Fig. 2(b), the visibility of the peaks is almost exactly mirrored about $p_\parallel = 0$ (black line) as illustrated by the thin blue curve, an exact mirror image of Fig. 2(a), highlighting the quality of the ion (and electron) momentum measurement as well as the CEP stabilization over time. For intermediate phases (not shown here) the visibility of the peaks becomes progressively less pronounced and symmetric about $p_\parallel = 0$ for $\phi_{\mathrm{CEP}} = 0$, while maintaining their positions. The momenta ($p_\parallel$), where interference peaks occur in Fig. 2, are plotted in Fig. 3 (red full circles) and compared to the results of previous measurements for 25 fs, non-CEP-stabilized pulses (blue open circles) at 790 nm [12]. The latter structures have been intensively discussed in the literature and were found to be stable in position over large intensity ranges, clearly visible deep into the tunneling regime [12]. Obviously the slope of the progressive peaks in this experiment differs drastically from the 25 fs data, which are in excellent agreement with a square root Above threshold ionization (ATI)-like behavior (black curve) where the spacing between peaks corresponds to the photon energy, i.e., to 0.057 a.u. (790 nm). The spacing between the here-observed peaks, however, is much smaller pointing to the

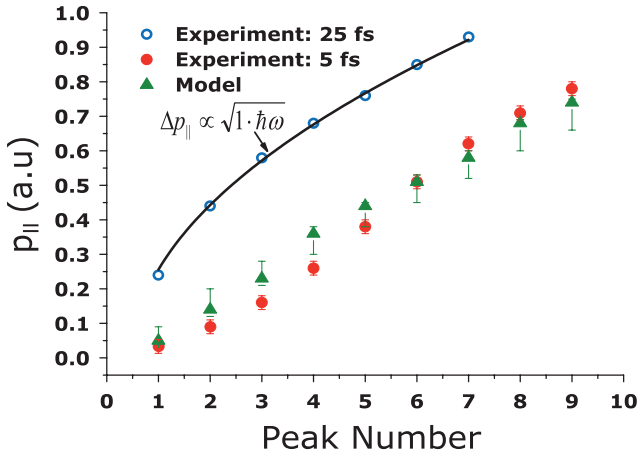

FIG. 3 (color). Positions of peaks in the parallel momentum $p_{\parallel}$ for 5 fs, 0.4 PW/cm^2 pulses at a phase of maximum asymmetry as extracted from Fig. 2 (red full circles). Blue open circles are from previous results for 25 fs, 0.6 PW/cm^2 (shaded area in Fig. 2) [12]. The black curve simulates a square-root ATI-like behavior. Green triangles: SFA model calculation (see text).

fact that in ultrashort pulses interferences emerging from wave-packet emission at the maxima of the oscillating electric field, i.e., at the carrier frequency corresponding to the photon energy of $\hbar\omega$, is widely suppressed. Instead a new, quite regular spacing emerges which now turns out to be nearly linear as a function of $p_{\parallel}$.

The 2D electron-momentum distribution, presented in Fig. 4 for a phase with maximum asymmetry, reveals quite

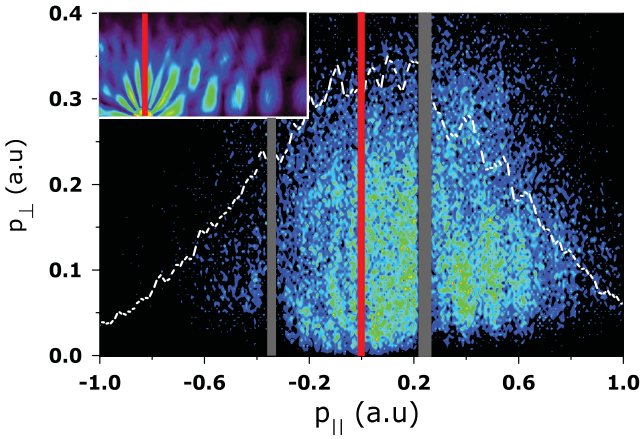

FIG. 4 (color). 2D electron-momentum distribution (linear scale) for a CE phase with maximum asymmetry. The x axis is the longitudinal momentum, the y axis is the momentum transverse to the polarization direction. The red line indicates the position of $p_{\parallel} = 0$. The projection onto the $p_{\parallel}$ axis is indicated as white dotted line. Events below the gray bar have been cut out since here the electron TOF is equal to an integer multiple of the cyclotron frequency of the electrons in the magnetic field of the reaction microscope and, accordingly, the transverse resolution diverges [8]. Inset : TDSE calculations for the ionization of He, with a Gaussian pulse, $I_0 = 0.3$ PW/cm^2, at 740 nm and FWHM ~2.7 fs.

parallel interference stripes along the momentum transverse to the polarization direction. Close to $p_{\parallel}$, $p_{\perp} = 0$ (red line) we see signatures of radial structures for $p_{\parallel} < 0$, indicating enhanced emission at certain angles, rapidly transforming into a more stripelike pattern for $p_{\parallel} > 0$. These spectra are in excellent qualitative agreement with recent theoretical predictions for two-cycle pulses [2], where the radial structures have been attributed to Coulumb-focusing, which also affects the relative positions of the stripelike fringes.

To interpret these results, we have developed a simple one-dimensional model based on SFA. The ionization in the model is confined to the most intense cycle of a sinelike pulse, and the electron motion is confined to the laser polarization axis only. The interference term arising from the superposition of the two quantum paths leading to the same momentum p (Fig. 1), referenced by their classical birth times $t_s (s = 1, 2)$, can be expressed by the p-dependent transition amplitude $T(p) = \sum_s C_s(p) e^{(i/2)p^2 t_s} e^{i\Phi_{\mathrm{IR}}(t_s)}$, where $\Phi_{\mathrm{IR}}(t_s) = \frac{1}{2} \times \int^{t_s} dt' \{2A(t')p + A^2(t')\}$, with $E(t) = -\frac{1}{c}\frac{\partial}{\partial t}A(t)$. Here $A(t)$ is the vector potential of the laser field and C_s, the amplitudes for wave packets created at t_s. Ignoring the contribution due to Coulomb effects, the final momentum distribution is interpreted as arising from the superposition of these two EWPs, shifted in time, and with additional phases, $\Phi_{\mathrm{IR}}(t_s)$, accounting for the Volkov action for a free electron in a strong laser field. It is evident that modulation in the momentum distributions strongly depends on the intensity and, hence, any comparison with the experiment would require us to obtain intensity averaged distributions. This was done by evaluating the above expressions for a pulse with a cos^2 intensity envelope with FWHM of 5 fs, $I_0 = 0.4$ PW/cm^2 at 740 nm, and averaged over intensities in a range of $\pm 6\%$.

In Fig. 3 the respective positions of the interference maxima, at a phase of maximum fringe asymmetry, are indicated as green triangles with uncertainty bars. The upper and lower ends of the bars indicate the peak positions for intensities with $\mp 6\%$ of I_0, respectively. For a given intensity (e.g., upper and lower bounds of the error bar) the evaluated peaks lie on a monotonic curve with a general behavior (slope) drastically different from the ATI-like structure, and nearly linear with $p_{\parallel}$. With increasing intensity the spacing between the fringes reduces, such that the interference maximum number 3 for the lower intensity overlaps with interference maximum number 4 of the higher intensity, thereby introducing some ambiguity in the counting procedure. This is reflected in the averaged results (green triangles) as a slight discontinuity between peaks number 3 and 4 in shifting from the lower to the upper end of the error bar. Actually, a similar behavior is observed in the experimental data between peaks number 4 and 5 (see also Fig. 2). Taking into account this unavoidable source of uncertainty in the experiment, we find excellent agreement between the experimental data and

the results of our simple model, exactly predicting the positions of the maxima within the given intensity fluctuations, distinctly different from any previous measurements where essentially ATI-like structures have been observed. One might be surprised about the quality of the prediction since recent theoretical investigations (see e.g., [13] and references therein), clearly emphasize the need for corrections to the SFA to more accurately describe electron-momentum distributions at low energies. In particular, it has been pointed out that the long range Coulomb potential changes the behavior of the asymmetry parameter such that the maximum asymmetry does not occur at phases $\phi_{\mathrm{CEP}} = \pm\pi$ as predicted by SFA but rather are found to be shifted by $\approx \pi/3$ in time-dependent Schrödinger equation (TDSE) as well as in semiclassical calculations taking the Coulomb potential into account. This shift being in general very sensitive on the pulse parameters was found to be quite universal for intensities between 10^{13} and 10^{14} W/cm^2. In the present analysis we have compared the experimental spectra at phases leading to maximum asymmetry to those of the SFA calculations at maximum asymmetry (for the interference fringes), such that we implicitly have accounted for an intensity (and electron momentum) independent effective phase shift of the experimental data due to the Coulomb potential. This might, at least partly, explain the excellent agreement between experiment and model calculations.

These results provide strong evidence that we have realized a true two-slit arrangement in time, where the slits are experimentally determined (different from earlier, pioneering measurements on two-slit interferences in the emitted x-ray energy during collisions [14] and also different from [15] where four slits were open at a time). Analyzing the FWHM, i.e., the visibility of one of the most prominent peaks (0.05 a.u for peak number 5 at $p_{\parallel} = 0.38$ a.u.) and relating it to the uncertainty of the birth time of the electron, we find an effective slit width $\Delta t < 20$ attoseconds. A similar analysis within our simple model indicates that the main sources of effective ''slit broadening'' are the intensity fluctuations in the pulse. In addition, other, smaller effects fading the fringe visibility are due to possible electron-momentum dependent phase shifts of the rescattered electron or a result of multiple recollisions since we certainly do not realize an ideal two-cycle laser pulse with zero field outside the two cycles. We have performed TDSE calculations in order to further substantiate our findings essentially reproducing the predictions in [2] and, thus, the salient features in the present data. We do observe, however, that the details of the patterns—as expected from any interference arrangement—do exhibit extreme sensitivity on the pulse shape, its intensity and duration on a level not controllable in this pioneering experiment. Moreover, the exact format of the screened He scattering potential plays a crucial role which will be the subject of a more detailed forthcoming analysis. Nevertheless, for demonstration we show one example of a TDSE result in the inset of Fig. 4.

With further progress in the control of the laser pulses or by monitoring the electric field through attosecond streaking we might rapidly proceed towards a situation that we can compare the experimental results to theoretical predictions on a level of being reliably sensitive on the scattering potential chosen in the calculation. In addition, the phase shifts in the spectra from different target atoms or molecules compared to the spectra from a suitable reference atom or molecule could be used to gain information on the atomic or molecular potential. Thus 3D momentum imaging of the interference of the rescattered, modulated EWP with an unaffected, directly launched EWP has the potential to obtain unprecedented information on the ultrashort time electron dynamics, on the details of the scattering potential, especially interesting if one considers molecules, as well as on the ultrashort response of the bound part of the many-electron wave function. In essence, the recolliding part of the wave-packet will, on the time scale of less than 20 attoseconds, certainly not see a static potential, but a dynamic electron cloud moving on the same time scale, such that one might become sensitive on the attosecond correlated motion of the bound electron(s). In the present case this process is particularly intriguing, since we split the two-electron wave function, interfere it with itself, and inspect the result in the single ionization channel.

We gratefully acknowledge numerous discussions with A. Voitkiv decisively helping in the interpretation of the data. We thank Ferenc Krausz and Karl-Ludwig Kompa for fruitful discussions and some specialized equipment. We are also grateful for support by the Max-Planck society and the DFG through the Emmy-Noether program and the Cluster of Excellence: Munich Center for Advanced Photonics.

[1] M. Spanner *et al.*, J. Phys. B **37**, L243 (2004).
[2] D. G. Arbó, E. Persson, and J. Burgdörfer, Phys. Rev. A **74**, 063407 (2006).
[3] J. Itatani *et al.*, Nature (London) **432**, 867 (2004).
[4] S. Baker *et al.*, Science **312**, 424 (2006).
[5] M. Okunishi *et al.*, Phys. Rev. Lett. **100**, 143001 (2008).
[6] T. Remetter *et al.*, Nature Phys. **2**, 323 (2006).
[7] J. Mauritsson *et al.*, Phys. Rev. Lett. **100**, 073003 (2008).
[8] J. Ullrich *et al.*, Rep. Prog. Phys. **66**, 1463 (2003).
[9] M. Schultze *et al.*, New J. Phys. **9**, 243 (2007).
[10] F. Lindner *et al.*, Phys. Rev. Lett. **92**, 113001 (2004).
[11] G. G. Paulus *et al.*, Phys. Rev. Lett. **91**, 253004 (2003).
[12] A. Rudenko *et al.*, J. Phys. B **37**, L407 (2004).
[13] D. B. Miloševic *et al.*, J. Phys. B **39**, R203 (2006).
[14] I. Tserruya *et al.*, Phys. Rev. Lett. **50**, 30 (1983).
[15] F. Lindner *et al.*, Phys. Rev. Lett. **95**, 040401 (2005).